

Two-band superconductivity with unconventional pairing symmetry in HfV_2Ga_4

A. Bhattacharyya,^{1,*} P. P. Ferreira,^{2,†} F. B. Santos,³ D. T. Adroja,^{4,5,‡} J. S. Lord,⁴ L. E. Correa,³ A. J. S. Machado,³ A. L. R. Manesco,^{2,6} and L. T. F. Eleno^{2,§}

¹*Department of Physics, Ramakrishna Mission Vivekananda Educational and Research Institute, Belur Math, Howrah 711202, West Bengal, India*

²*Computational Materials Science Group (ComputEEL),*

Escola de Engenharia de Lorena, Universidade de São Paulo (EEL-USP),

Materials Engineering Department (Demar), Lorena – SP, Brazil

³*Escola de Engenharia de Lorena, Universidade de São Paulo (EEL-USP),*

Materials Engineering Department (Demar), Lorena – SP, Brazil

⁴*ISIS Facility, Rutherford Appleton Laboratory, Chilton, Didcot, Oxon, OX11 0QX, United Kingdom*

⁵*Highly Correlated Matter Research Group, Physics Department,*

University of Johannesburg, Auckland Park 2006, South Africa

⁶*Kavli Institute of Nanoscience, Delft University of Technology, Delft, The Netherlands*

(Dated: November 10, 2021)

In this letter, we have examined the superconducting ground state of the HfV_2Ga_4 compound using resistivity, magnetization, zero-field (ZF) and transverse-field (TF) muon-spin relaxation and rotation (μSR) measurements. Resistivity and magnetization unveil the onset of bulk superconductivity with $T_c \sim 3.9$ K, while TF- μSR measurements show that the temperature dependence of the superfluid density is well described by a nodal two-gap $s+d$ -wave order parameter model. In addition, ZF muon relaxation rate increases with decreasing temperature below 4.6 K, indicating the presence of weak spin fluctuations. These observations suggest an unconventional multiband nature of the superconductivity possibly arising from the distinct d -bands of V and Hf ions with spin fluctuations playing an important role. To better understand these findings, we carry out first-principles electronic-structure calculations, further highlighting that the Fermi surface consists of multiple disconnected sheets with very different orbital weights and spin-orbit coupling, bridging the way for a nodal multiband superconductivity scenario. In this vein, therefore, HfV_2Ga_4 -family stands out as an open avenue to novel unexplored unconventional superconducting compounds, such as ScV_2Ga_4 and ZrV_2Ga_4 , and other many rare earths based materials.

PACS numbers: 71.20.Be, 76.75.+i

Unconventional superconducting materials have attracted considerable interest over the last decades due to their extremely rich physics and emerging breakthrough properties [1, 2]. In such materials, the superconducting state transcends the BCS-like signatures, as well as the isotropic s -wave pairing symmetry of the gap structure. Instead, a complex interaction framework among electrons, the crystal lattice, and spin-orbital fluctuations are established as the possible mediation mechanism of the Cooper pairs [3]. HfV_2Ga_4 is a newly discovered superconducting compound with a critical temperature (T_c) of ≈ 3.9 K that crystallizes in the tetragonal body-centered prototype YbMo_2Ga_4 [1]. Substantial deviations of the temperature dependence of upper and lower critical fields from the expected Werthamer-Helfand-Hohenberg (WHH) formula [4] has led the authors to argue in favor of the presence of two superconducting gaps in the Fermi surface [1]. Later, first-principles electronic-structure calculations revealed the presence of electrons occupying very distinct bands at the Fermi level in the presence of spin-orbit coupling (SOC) effects [11]. Also, a substantial elastic anisotropy regime, due to the presence of extended linear vanadium chains in the structure [7], indicates the feasibility of multiband superconductivity and the manifestation of possible un-

conventional properties.

In this Letter, we present unambiguous evidence of two-gap nodal superconductivity in HfV_2Ga_4 using transverse (TF) muon spin rotation (μSR) measurement. However, in opposition to what is generally accepted in previous experimental and theoretical attempts, we have discovered an unconventional superconducting order parameter with $s+d$ -wave pairing symmetry and spin fluctuations traces. These experimental findings are further supported by density functional theory (DFT) calculations. Therefore, HfV_2Ga_4 could represent a novel family of unconventional superconductors, going beyond Fe-based compounds, heavy-fermions, non-centrosymmetric systems, and other known classes [1–3]. Thus, several compounds within the HfV_2Ga_4 -family, such as ScV_2Ga_4 and ZrV_2Ga_4 [7, 11], stand out as an open avenue to further investigate unconventional superconducting properties using various experiments and theoretical models.

For the present μSR study a high-quality polycrystalline sample of HfV_2Ga_4 was prepared by arc melting of the stoichiometric amount of hafnium, vanadium, and gallium on a water-cooled Cu crucible in a high-purity Ar atmosphere, the arc-melted pellet was encapsulated in an evacuated quartz ampoule and heated up to 800 °C and kept at that temperature for one week, then

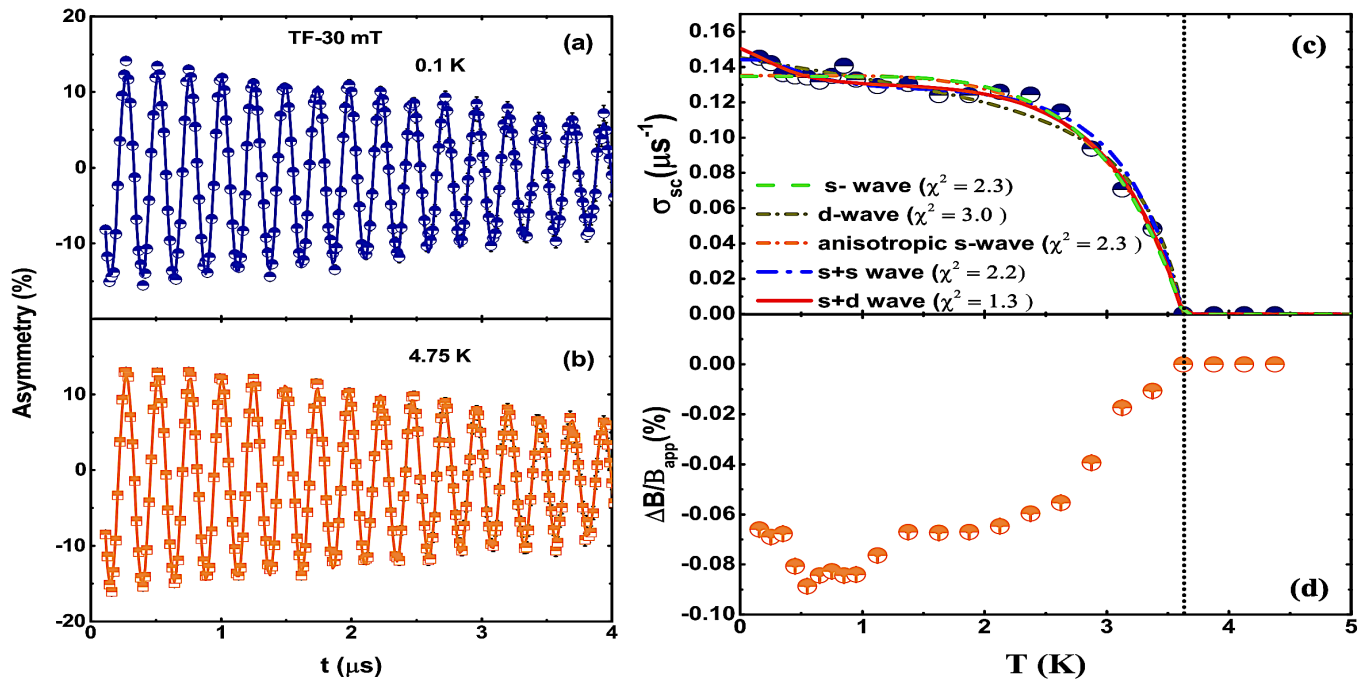


FIG. 1. Representative TF- μ SR asymmetry spectra in the low time region collected at (a) at $T = 0.1$ K and (b) at $T = 4.75$ K (i.e. below and above T_C) in an applied magnetic field of 30 mT. (c) Represent the $\sigma_{sc}(T)$ data in field cooling mode with fits using various gap models. The dash green line shows the fit using an isotropic single-gap s -wave model, the solid red line and dash-dotted blue line show the fit to a two-gap model, $s+d$ -wave and $s+s$ -wave, respectively. The orange dash-dotted line shows the fit using an anisotropic s -wave model and the dash-dotted purple line shows the fit using d -wave model. (d) Temperature dependence of the normalized internal field from the sample.

quenched in cold water [1]. Magnetotransport measurements were performed using a VSM-PPMS EverCool II from Quantum Design. A powdered sample of HfV_2Ga_4 was used for the μ SR experiments, which were carried out on the MUSR spectrometer at the ISIS Pulsed Neutron and Muon Source of Rutherford Appleton Laboratory, U.K. The sample was placed on a silver holder (99.999%) using GE-varnish, which was loaded in a dilution refrigerator operating between 0.1 K and 4.75 K. Zero-field (ZF) and transverse field (TF)- μ SR measurements were performed at different temperatures between 0.1 K and 4.75 K. For ZF- μ SR measurement, an active compensation system was used to cancel any stray magnetic fields at the sample space to a level of $\sim 10^{-4}$ mT. ZF- μ SR measurement is beneficial to identify the spontaneous internal field associated with time-reversal symmetry breaking [2]. TF- μ SR measurements were carried out in the presence of an external magnetic of 30 mT, which is well above the lower critical field ($\mu_0 H_{c1} = 1.2$ mT), and well below the upper critical field ($\mu_0 H_{c2} = 1.1$ T) of HfV_2Ga_4 . The experimental data were analyzed using the WiMDA software [9].

Santos *et al.* [1] recently reported superconductivity on HfV_2Ga_4 at $T_C = 3.9$ K, in which the upper and lower critical fields show unusual dependence with reduced temperature (T/T_C), suggesting strong devia-

tions from the conventional BCS behavior. This type of unusual behavior is also seen for other materials, such as $\text{Cu}_{0.3}\text{ZrTe}_{2-y}$ [10], fluorine doped NdFeAsO [11], FeSe [12], $\text{SmFeAs}_{0.09}\text{F}_{0.01}$, $\text{Ba}_{0.6}\text{K}_{0.4}\text{Fe}_2\text{As}_2$ [13, 14] and MgB_2 [15]. To clarify the microscopic characteristics and superconducting gap structure of HfV_2Ga_4 , TF- μ SR measurements were carried in the mixed superconducting state. First, we applied an external magnetic field of 30 mT above T_C , followed by colling down to 0.1 K. The TF- μ SR asymmetry spectra were collected at various temperatures up to T_C . Figs. 1(a)-(b) exhibit two representative TF- μ SR spectra collected at $T = 4.75$ K and 0.1 K in $H = 30$ mT. The asymmetry spectra at 0.1 K show faster relaxation compared to 4.75 K data as a result of the development of the flux line lattice below T_C . The time evolution of the μ SR asymmetry can be modeled by $A_{\text{TF}}(t) = A_1 \cos(\gamma_\mu B_1 t + \Phi) \exp(-\frac{\sigma^2 t^2}{2}) + A_{bg} \cos(\gamma_\nu B_{bg} t + \Phi)$ [16–19], where A_1 and A_{bg} describe the initial asymmetries belonging to the sample and silver holder contributions, individually, with A_{bg} not undergoing any depolarization; B_1 and B_{bg} are the internal fields from the sample and from the sample holder, respectively. $\gamma_\nu/2\pi = 135.53$ MHz/T is the muon gyromagnetic ratio; Φ is the initial phase; and σ is a Gaussian muon spin relaxation rate. The flux line lattice related muon relaxation can be extracted by subtracting the nuclear contribution according

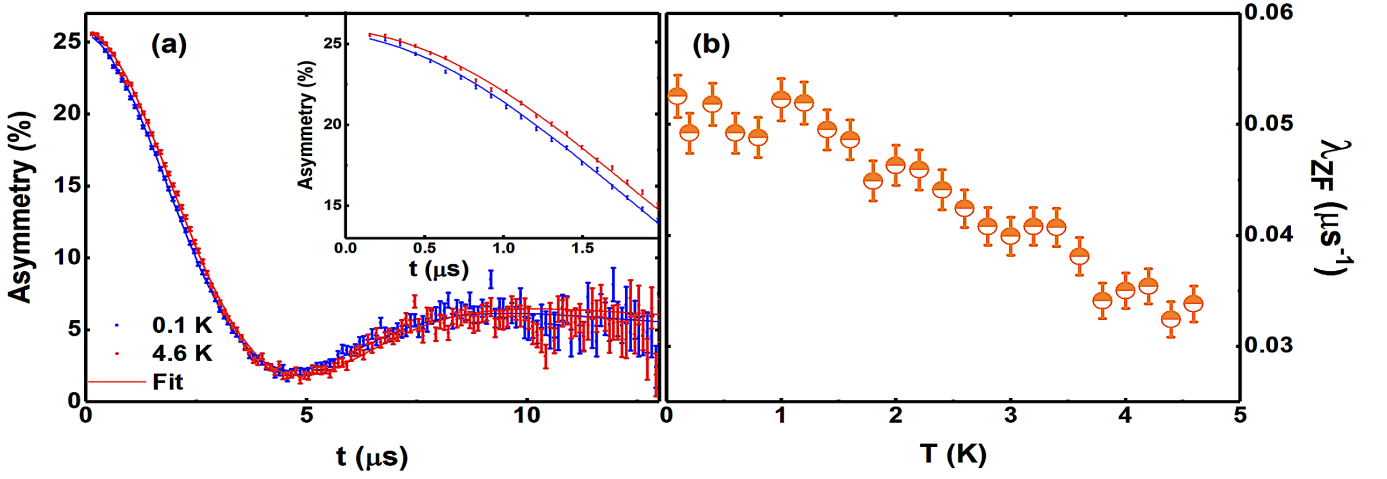


FIG. 2. (a) Represent the ZF- μ SR spectra for HfV_2Ga_4 at 0.1 K and 4.6 K. The solid lines are fits to the data, as described in the text. The inset shows the asymmetry data at lower time. (b) shows the temperature dependence of the relaxation rate $\lambda_{ZF}(T)$, which intimate the presence of spin fluctuations.

$\sigma_{sc} = \sqrt{\sigma^2 - \sigma_n^2}$, where σ_n is the nuclear magnetic dipolar contribution which is temperature independent and was obtained from spectra measured above T_C . By fitting the spectra at 4.75 K we obtained $\sigma_n = 0.35 \mu\text{s}^{-1}$. Considering that σ_{sc} is linked to the magnetic penetration depth (λ) by $\sigma_{sc} \approx 1/\lambda^2$, the superconducting gap symmetry can be determined from the temperature dependence of $\sigma_{sc}(T)$. The temperature-dependent of magnetic penetration depth was analyzed employing different models, generally described by $\frac{\sigma_{sc}(T)}{\sigma_{sc}(0)} = \frac{\lambda^{-2}(T)}{\lambda^{-2}(0)} = 1 + \frac{1}{\pi} \int_0^{2\pi} \int_{\Delta(T,\phi)}^{\infty} \left(\frac{\partial f}{\partial E} \right) \frac{E dE d\phi}{\sqrt{E^2 - \Delta(T,\phi)^2}}$ [20, 21], where Δ is an angle-dependent gap function, $f = [1 + \exp(-E/k_B T)]^{-1}$ is the Fermi function, and the integration signifies an average across the Fermi surface. The gap is expected to follow the function $\Delta(T) = \Delta_0 \delta(T/T_C) g(\phi)$, where Δ_0 is the maximum gap value at zero temperature and $g(\phi)$ is the angular dependence of the gap, equal to 1 and $\cos(2\phi)$ for an s - and d -wave model, respectively. Here ϕ is the azimuthal angle. The superconducting gap symmetry is expected to follow $\delta(T/T_C) = \tanh[1.82[1.018(T_C/T - 1)]^{0.51}]$ [22, 23]. This gap function is sufficiently precise to explain the temperature dependency at any coupling strength.

The $\lambda^{-2}(T)$ data were fitted based on five different gap models (a) an isotropic s -wave gap, (b) an isotropic $s+s$ -wave, (c) anisotropic s -wave, (d) a d -wave line node and (e) a nodal $s+d$ -wave, as shown in Fig. 1(c). The estimated fit parameters are given in the Supplemental Material [24] in Table I. Further, the diamagnetic signal observed below T_C can be seen through the decrease in the internal field below T_C as shown in Fig. 1(d). From the fits presented in Fig. 1(c) it is obvious that the isotropic s -wave, anisotropic s -wave, d -wave models do not fit the data as they give a high value of good-

ness of fit χ^2 . Contrariwise, two-gap models using the isotropic $s+s$ -wave and a nodal $s+d$ -wave show good fits to the $\lambda^{-2}(T)$ data. Furthermore the low T upturn can be best fitted with a nodal $s+d$ -wave model with a minimum value of $\chi^2 = 1.3$. The estimated parameters for the nodal $s+d$ -wave model show one larger gap $2\Delta_1(0)/k_B T_C = 6.27 \pm 0.2$ (meV), which is larger than the value of 3.53 as expected for conventional BCS gap and another smaller gap $2\Delta_2(0)/k_B T_C = 1.14 \pm 0.1$ (meV). The smaller gap is a nodal gap for the $s+d$ -wave model. Moreover, the large gap value indicates the presence of strong coupling superconductivity in HfV_2Ga_4 . The parameters obtained from the fit to the $\sigma_{sc}(T)$ data of HfV_2Ga_4 using different gap models is presented in the Supplemental Material [24]. The multigap features are usually seen in iron-based superconductors, $\text{Ba}_{1-x}\text{K}_x\text{Fe}_2\text{As}_2$ [25, 26], cuprate superconductors [27, 28] also in $\text{Bi}_4\text{O}_4\text{S}_3$ [29]. Following the method described in Ref. [31], we determined the values of $\lambda_L(0) = 797(4)$ nm for $s+d$ wave fit, $n_s = 6.78(9) \times 10^{25}$ carriers m^{-3} , and $m^* = 1.528(2)m_e$ respectively, for HfV_2Ga_4 . For a detail calculations see the Supplemental Material [24].

To examine the fundamental issue of the presence of time-reversal symmetry (TRS) breaking or spin fluctuations in HfV_2Ga_4 , we did ZF- μ SR measurements. This technique is extremely helpful to identify the tiny spontaneous magnetic fields below T_C . In the case of conventional superconductors, there is no change in the ZF muon relaxation rate (λ_{ZF}) below T_C . λ_{ZF} increases with decrease in temperature at T_C if TRS is broken. Fig. 2(a) shows the ZF- μ SR signal at 4.6 K and 0.1 K. The ZF- μ SR signal could be best described by a combined Lorentzian and Gaussian Kubo-Toyabe relaxation function: $A_{ZF}(t) = A_2 A_{KT}(t) e^{-\lambda_{ZF} t} + A_{bg}$, here $A_{KT}(t) = [\frac{1}{3} + \frac{2}{3}(1 - \sigma_{KT}^2 t^2) \exp(-\frac{\sigma_{KT}^2 t^2}{2})]$, is known as

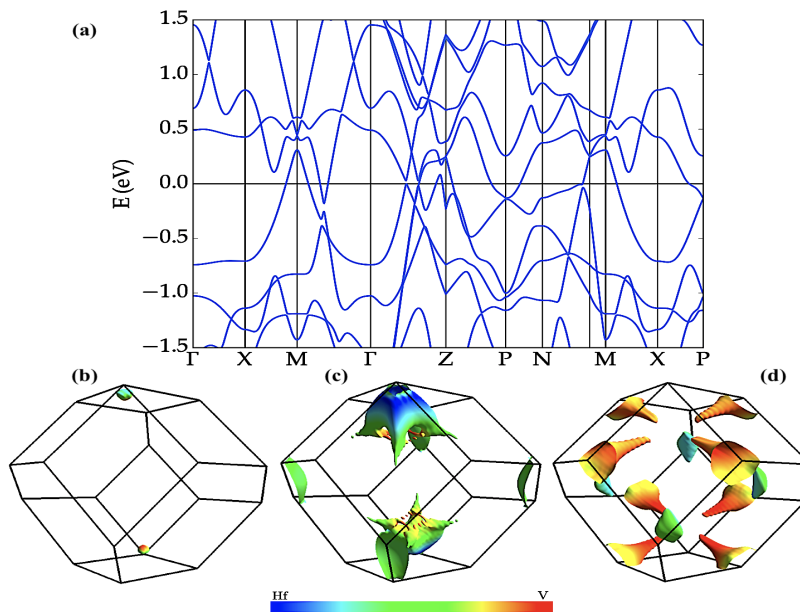


FIG. 3. (Upper panel) Electronic bands along a selected path in the first BZ of HfV_2Ga_4 . The Fermi energy (E_F) is set at 0.0 eV. (Lower panel) Hf- and V-d orbital character contribution to electronic states projected over the three distinct Fermi surface sheets.

the Gaussian Kubo-Toyabe function, A_2 and A_{bg} represent the asymmetry contribution from sample and silver holder, respectively. The resulting fit parameter is shown in Fig. 2(b). It is interesting to note that $\lambda_{ZF}(T)$ increases with decreasing temperature, suggesting the presence of spin-fluctuation in HfV_2Ga_4 . Furthermore, the fits to the ZF data give $\sigma_{KT} = 0.368(5) \mu\text{s}^{-1}$ and $\lambda_\mu = 0.0525(5) \mu\text{s}^{-1}$ at 0.1 K and $\sigma_{KT} = 0.368(5) \mu\text{s}^{-1}$ and $\lambda_\mu = 0.0337(6) \mu\text{s}^{-1}$ at 4.6 K.

Analysis of band-structure and Fermi surface of the HfV_2Ga_4 compound can provide a suitable baseline from which to raise some phenomenological hypothesis of the mechanisms involved in such unconventional superconductivity shown by the experimental evidence presented in this letter. Therefore, optimized first-principles calculations were carried out in the framework of the Kohn-Sham scheme within the Density Functional Theory (DFT) [32, 33], performed within the pseudopotential approach in the Perdew-Burke-Ernzerhof (PBE) generalized gradient approximation [34, 35] as implemented in Quantum ESPRESSO [36, 37] and support by auxiliary codes [38, 39].

Fig. reffig:fermisurface(a) shows the band-structure through high-symmetry points in the first Brillouin zone (BZ) [40]. Multiple distinct bands are crossing the Fermi energy (E_F), with very contrasting V-d and Hf-d characters. Other atomic orbital contributions to the electronic density in the vicinity of the E_F are negligible. The obtained results are in great agreement with previous electronic-structure calculations [11], except for the presence of an additional band in the Fermi level (resulting in

a very small quasi-spheric hole-pocket around the Z point in the Fermi surface). Additionally, Fig. 3(b-d) presents the projected-orbital Fermi surface with a color scheme for each irreducible representation. The reddish regions indicate a substantial contribution of V-d orbitals, which dictate the density of states (DOS) at the Fermi level; the bluish ones represent a major character derived from Hf-d orbitals; while the greenish branches depict a strong hybridization between these two states, as indicated by the color bar scale.

The Fermi surface consists of multiple tridimensional disconnected sheets, bridging the way for a multiband superconductivity scenario: (a) a minor hybridized hole sphere next to the Z point; (b) a quasi-hyperbolic paraboloid with hole carriers that develops around the M point with substantial admixture of Hf-d and V-d orbitals, in the midpoint of the line that connects the two rhombuses (which we will call *horse-saddle*), plus a very complex hole-like surface around the Z point composed mainly by Hf-d character with a slight degree of V-d (*jellyfish*); (c) and multiple V-d electron cone-shaped pockets around the P point (*seashell*), together with small electron-pockets saddled within the BZ along the M- Γ high-symmetry line.

Such hole bands with a predominant Hf-derived character are deeply sensitive against spin-orbit interactions, as opposed to V-d bands, which, in turn, play a crucial role in the low-energy electronic states [11]. This fermiology, with very distinct disconnected pockets, in the sense of their orbital weight contribution and, hence, their effective spin-orbit coupling, favors the condensation of

pairs with different superconducting order parameters. Since *jellyfish*-pockets have a strong Hf-d character, we could expect the emergence of pair states with non-zero angular momentum and strong angular anisotropy, resulting in an even-parity momentum-dependent order parameter. On the other hand, the negligible effect of SOC in V bands favors the emergence of conventional *s*-wave pairing. This interpretation supports the experimental *s* + *d*-wave symmetry as founded. Moreover, the weighting factor of 0.57 to *s*-wave pairing is attributed to the higher contribution of V states on the DOS at the Fermi level, residing mainly at the *seashell*-pockets, and a lower *d*-wave character coming from those Hf-derived structures.

On the other hand, repulsive interactions between the sheets, driven by spin fluctuations, for instance, are unexpected due to the complex nature of the fermiology. However, the *jellyfish*- and *horse-saddle*-pockets will take advantage of hole doping, increasing the SOC effects on the low-energy states, at the same time that *seashell*-pockets will gradually decrease (see the Supplemental Material [24]), paving the way for discontinuous sign change of the order parameter phase and spin fluctuations by the enlargement of possible nearly induced nesting instabilities [41–44]. This mechanism becomes relevant in our context since Ga-deficient HfV₂Ga₄ samples can, in a first approximation, effectively decrease the chemical potential of occupied states by a few meV, promoting such features. Also, hole doping promotes an increase in the density of states, favoring electronic correlations, and contributing to spontaneous symmetry breaking mechanisms. Indeed, nearly nested Fermi surface pockets and the anisotropic gap function support the enhanced pairing strength observed in μ SR measurements ($2\Delta_1/k_B T_c = 6.27$) [45–47]. Therefore, Ga-deficiency can be imperative to the unconventional superconductivity of HfV₂Ga₄, which seems to be unique, and high-quality single crystals, with systematic doping content, are urgently required to investigate the superconducting state further and to confirm the proposed hypothesis.

In summary, we have examined the superconducting state of HfV₂Ga₄ utilizing magnetotransport, μ SR, and numerical band-structure calculations. The temperature dependence of the magnetic penetration depth, $\lambda^{-2}(T)$, is better fitted to a nodal two-gap *s*+*d*-wave model than a single gap isotropic *s*-wave, anisotropic *s*-wave or *d*-wave models, suggesting unconventional superconductivity in HfV₂Ga₄. The large value of gap to T_c ratio, $2\Delta_1(0)/k_B T_c = 6.27 \pm 0.2$, obtained from the nodal *s*+*d*-wave gap, is larger than 3.53, expected for conventional BCS superconductors, indicating the presence of strong coupling superconductivity in HfV₂Ga₄. The decrease in ZF relaxation rate with temperature indicates the presence of spin fluctuations in the superconducting state of HfV₂Ga₄. In addition, *ab initio* calculations suggest that there are electrons derived from multiple distinct bands

in disconnected sheets of the Fermi surface, in agreement with the experimental evidence of two-gap superconductivity for HfV₂Ga₄, and the momentum-dependent SOC interactions may be a theoretical starting point to elucidate the appearance of nodal superconductivity.

We want to acknowledge Mr. Kartik Panda for helping MUSR data analysis and Prof. A. M. Strydom for interesting discussions. AB would like to acknowledge the Department of Science and Technology (DST) India, for an Inspire Faculty Research Grant (DST/INSPIRE/04/2015/000169), and the UK-India Newton grant for funding support. DTA would like to thank the Royal Society of London for the UK-China Newton funding and the Japan Society for the Promotion of Science for an invitation fellowship. FBS, PPF, LEC, AJSM, ALRM, and LTFE gratefully acknowledge the financial support of the Brazilian agencies Conselho Nacional de Desenvolvimento Científico e Tecnológico (CNPq) under Grants No. 302149/2017-1 and 431868/2018-2, and Fundação de Amparo à Pesquisa do Estado de São Paulo (FAPESP) under Grants No. 2016/11774-5, 2016/11565-7, 2016/10167-8, 2018/08819-2, 2018/10835-6, 2018/20546-1, 2019/05005-7, and 2019/07082-9.

* amitava.bhattacharyya@rkmvu.ac.in

† pedroferreira@usp.br

‡ devashibhai.adroja@stfc.ac.uk

§ luizeleno@usp.br

- [1] D. J. Scalapino, *Reviews of Modern Physics* **84**, 1383 (2012).
- [2] G. Stewart, *Advances in Physics* **66**, 75 (2017).
- [3] M. Norman, arXiv preprint arXiv:1302.3176 (2013).
- [4] N. R. Werthamer, E. Helfand, and P. C. Hohenberg, *Phys. Rev.* **147**, 295 (1966).
- [5] F. B. Santos, L. E. Correa, B. S. de Lima, O. V. Cigarroa, M. S. da Luz, T. W. Grant, Z. Fisk and A. J. S. Machado, *Phys. Lett. A* **382**, 1065 (2018).
- [6] P. Ferreira, F. Santos, A. Machado, H. Petrilli, and L. Eleno, *Phys. Rev. B* **98**, 045126 (2018).
- [7] P. Ferreira, T. Dorini, F. Santos, A. Machado, and L. Eleno, *Materialia* **4**, 529 (2018).
- [8] J. E. Sonier, J. H. Brewer, and R. F. Kiefl, *Rev. Mod. Phys.* **72**, 769 (2000).
- [9] F. L. Pratt, *Physica B* **289-290**, 710 (2000).
- [10] A.J.S. Machado, N.P. Baptista, B.S. De Lima, N. Chaia, T.W. Grant, L.E. Correa, S.T. Renosto, A.C. Scaramussa, R.F. Jardim, M.S. Torikachvili, J.A. Aguiar, O.C. Cigarroa, L.T.F. Eleno, Z. Fisk, *Phys. Rev. B* **95**, 144505 (2017).
- [11] A. Adamski, C. Krellner, M. Adbel-Hafiez, *Phys. Rev. B* **95**, 100503 (2017).
- [12] M. Abdel-Hafiez, J. Ge, A.N. Vasiliev, D.A. Chareev, J. Van De Vondel, V.V. Moshchalkov, A.V. Silhanek, *Phys. Rev. B*, **88**, 174512 (2013).
- [13] C. Ren, Z.S. Wang, H.Q. Luo, H. Yang, L. Shan, H.H. Wen, *Physica C, Supercond. Appl.* **469**, 599 (2009).

- [14] C. Ren, Z.S. Wang, H.Q. Luo, H. Yang, L. Shan, H.H. Wen, *Phys. Rev. Lett.* **101**, 257006 (2008).
- [15] S. L. Li, H. H. Wen, Z. W. Zhao, Y. M. Ni, Z. A. Ren, G. C. Che, H. P. Yang, Z. Y. Liu, Z. X. Zhao, *Phys. Rev. B* **64**, 94522 (2001).
- [16] A. Bhattacharyya, D. T. Adroja, M. Smidman, and V. K. Anand, *Sci. China-Phys. Mech. Astron.* **61**, 127402 (2018).
- [17] D. T. Adroja, A. Bhattacharyya, P. K. Biswas, M. Smidman, A. D. Hillier, H. Mao, H. Luo, G. H. Cao, Z. Wang and C. Wang, *Phys. Rev. B* **96**, 144502 (2017).
- [18] A. Bhattacharyya, D. T. Adroja, K. Panda, S. Saha, T. Das, A. J. S. Machado, T. W. Grant, Z. Fisk, A. D. Hillier and P. Manfrinetti, *Phys. Rev. Lett.* **122** 1477001 (2019).
- [19] A. Bhattacharyya, D. T. Adroja, J. Quintanilla, A. D. Hillier, N. Kase, A. M. Strydom, and J. Akimitsu, *Phys. Rev. B* **91** 060503 (2015).
- [20] R. Prozorov, and R. W. Giannetta, *Supercond. Sci. Technol.* **19**, R41 (2006).
- [21] D. T. Adroja, A. Bhattacharyya, M. Telling, Y. Feng, M. Smidman, B. Pan, J. Zhao, A. D. Hillier, F. L. Pratt, and A. M. Strydom, *Phys. Rev. B* **92**, 134505 (2015).
- [22] G. Pang, M. Smidman, W. Jiang, J. Bao, Z. Weng, Y. Wang, L. Jiao, J. Zhang, G. Cao, and H. Yuan, *Phys. Rev. B* **91**, 220502 (2015).
- [23] J. F. Annett, *Adv. Phys.* **39**, 83-126 (1990).
- [24] See Supplemental Material for more information on the crystal structure, resistivity and magnetization, and Uemura Plot.
- [25] D. V. Evtushinsky, D. S. Inosov, V. B. Zabolotnyy, M. S. Viazovska, R. Khasanov, A. Amato, H. -H. Klauss, H. Luetkens, Ch Niedermayer, G. L. Sun, V. Hinkov, C. T. Lin, A. Varykhalov, A. Koitzsch, M. Knupfer, B. Chner, A. A. Kordyuk, and S. V. Borisenko, *New J. Phys.*, **11**, 055069 (2009).
- [26] R. Khasanov, D.V. Evtushinsky, A. Amato, H.-H. Klauss, H. Luetkens, Ch. Niedermayer, B. Buchner, G. L. Sun, C. T. Lin, J. T. Park, D. S. Inosov, and V. Hinkov, *Phys. Rev. Lett.* **102**, 187005 (2009).
- [27] R. Khasanov, S. Strassle, D. Di Castro, T. Masui, S. Miyasaka, S. Tajima, A. Bussmann-Holder, and H. Keller, *Phys. Rev. Lett.* **99**, 237601 (2007).
- [28] B. Keimer, S. A. Kivelson, M. R. Norman, S. Uchida, and J. Zaanen, *Nature* **518**, 179 (2015).
- [29] P. K. Biswas, A. Amato, C. Baines, R. Khasanov, H. Luetkens, Hechang Lei, C. Petrovic, and E. Morenson, *Phys. Rev. B* **58**, 224515 (2013).
- [30] E. H. Brandt, *Phys. Rev. B* **68**, 054506 (2003).
- [31] A. Hillier and R. Cywinski, *Appl. Magn. Reson.* **13**, 95 (1997).
- [32] P. Hohenberg and W. Kohn, *Phys. Rev.* **136**, B864 (1964).
- [33] W. Kohn and L. J. Sham, *Phys. Rev.* **140**, A1133 (1965).
- [34] J. P. Perdew, K. Burke, and M. Ernzerhof, *Phys. Rev. Lett.* **77**, 3865 (1996).
- [35] A. Dal Corso, *Computational Materials Science* **95**, 337 (2014).
- [36] P. Giannozzi, S. Baroni, N. Bonini, M. Calandra, R. Car, C. Cavazzoni, D. Ceresoli, G. L. Chiarotti, M. Cococcioni, I. Dabo, et al., *J. Phys. Cond. Matter* **21**, 395502 (2009).
- [37] P. Giannozzi, O. Andreussi, T. Brumme, O. Bunau, M. B. Nardelli, M. Calandra, R. Car, C. Cavazzoni, D. Ceresoli, M. Cococcioni, et al., *J. Phys. Cond. Matter* **29**, 465901 (2017).
- [38] M. Kawamura, *Computer Physics Communications* **239**, 197 (2019).
- [39] A. Kokalj, *Journal of Molecular Graphics and Modelling* **17**, 176 (1999).
- [40] W. Setyawan and S. Curtarolo, *Computational materials science* **49**, 299 (2010).
- [41] K. Kuroki and R. Arita, *Phys. Rev. B* **64**, 024501 (2001).
- [42] I. Mazin, D. J. Singh, M. Johannes, and M.-H. Du, *Phys. Rev. Lett.* **101**, 057003 (2008).
- [43] K. Kuroki, S. Onari, R. Arita, H. Usui, Y. Tanaka, H. Kontani, and H. Aoki, *Phys. Rev. Lett.* **101**, 087004 (2008).
- [44] D. J. Singh, *New Journal of Physics* **14**, 123003 (2012).
- [45] K. Terashima, Y. Sekiba, J. Bowen, K. Nakayama, T. Kawahara, T. Sato, P. Richard, Y. -M. Xu, L. Li, G. Cao, et al., *Proceedings of the National Academy of Sciences* **106**, 7330 (2009).
- [46] P. Monthoux and D. Scalapino, *Phys. Rev. B* **50**, 10339 (1994).
- [47] C.-H. Pao and N. Bickers, *Phys. Rev. Lett.* **72**, 1870 (1994).

**SUPPLEMENTAL MATERIAL: TWO-BAND
SUPERCONDUCTIVITY WITH
UNCONVENTIONAL PAIRING SYMMETRY IN
HFV₂Ga₄**

Crystal Structure, Resistivity, and Magnetization

Fig. 4(a) manifests a representative XRD pattern along with refinement which confirms the single-phase nature of HfV₂Ga₄ sample. It crystallizes in the YbMo₂Al₄ prototype tetragonal structure [1] with space group *I4/mmm*, no 139. The inset of Fig. 4(a) displays a schematic illustration of tetragonal unit cell where Hf (gray), V (blue), and Ga (red) sites are at the $2a$ (0, 0, 0), $4d$ (0, $\frac{1}{2}$, $\frac{1}{4}$), and $8h$ (0.303, 0.303, 0) Wyckoff positions, respectively. As shown in Fig. 4(b), the $\rho(T)$ data exhibit a metallic behavior down to the superconducting transition at $T_C = 3.9$ K. As shown in Fig. 4(c), magnetic susceptibility $\chi(T)$ data show T_C at 3.9 K, consistent with the value determined from $\rho(T)$ data.

TF- μ SR: Superconducting Parameters

The muon spin depolarization rate observed below T_C is linked to the magnetic penetration depth. For a triangular[2-5] lattice $\frac{\sigma_{sc}^2}{\gamma_\mu^2} = \frac{0.00371 \times \phi_0^2}{\lambda^4}$, where $\phi_0 = 2.07 \times 10^{-15}$ Tm², is the flux quantum number and $\gamma_\mu/2\pi = 135.5$ MHz T⁻¹, is the muon gyromagnetic ratio. Using London's theory [2] $\lambda_L^2 = \frac{m^* c^2}{4\pi n_s e^2}$, where $m^* = (1 + \lambda_{e-ph})m_e$ is the effective mass and n_s is the density of superconducting carriers. λ_{e-ph} is the electron-photon coupling constant that estimated using McMillans relation [6-8]: $\lambda_{e-ph} = \frac{1.04 + \mu^* \ln(\Theta_D/1.45T_C)}{(1 - 0.62\mu^*) \ln(\Theta_D/1.45T_C) - 1.04}$, here μ^* is the repulsive screened Coulomb parameter with a typical value of $\mu^* = 0.12$ and $\Theta_D = 416.3$ K, give $\lambda_{e-ph} = 0.528(2)$. As HfV₂Ga₄ is a type II superconductor, supposing that approximately all the normal states carriers (n_e) contribute to the superconductivity ($n_s \approx n_e$), the magnetic penetration depth λ , superconducting carrier density n_s , the effective-mass enhancement m^* have been estimated to be $\lambda_L(0) = 797(4)$ nm, $n_s = 6.78(9) \times 10^{25}$ carriers m⁻³, and $m^* = 1.528(2)m_e$ respectively, for HfV₂Ga₄.

Uemura Plot: Unconventional Superconductivity

Uemura plot [10] is crucial for classifying conventional and unconventional superconductors. In case of, Uemura classification scheme, which considers the correspondence between T_C and the effective Fermi temperature, T_F , determined from TF- μ SR measurement [9]. Uemura *et al.* suggested that exotic superconductors, i.e. high T_C

cuprates, heavy fermions, Chevrel phases and the organic superconductors, form a similar but different group, defined by a universal scaling of T_C with T_F such that $1/10 > (T_C/T_F) > 1/100$ as shown in Fig. 5. For conventional BCS superconductors $1/1000 > (T_C/T_F)$. The estimated value of $T_C/T_F = 3.9/460.97 = 0.00846$ for HfV₂Ga₄, which further suggest that HfV₂Ga₄ can be classified as an unconventional superconductor as shown in Fig. 5, according to Uemura's scheme [10].

First-principles calculations: Hole doping effect

Fig. 6(a-c) shows modified Fermi surfaces by lowering the chemical potential in HfV₂Ga₄ by a few meV. The figures simulate, in the rigid band approximation, the depletion of electrons in going from the calculated HfV₂Ga₄ compound to HfV₂Ga_{3.7}, as experimentally measured. The hole *jellyfish*- and *horse-saddle*-pockets will continually increase, favoring spin-orbit coupling, nesting regions, and correlation effects, whereas the electron *seashell*-pockets will gradually decrease. This hole doping can be reached, in a first approximation, utilizing Ga-deficiency control in HfV₂Ga₄ samples, considering the nature of Ga-Ga atomic bonding [11].

* amitava.bhattacharyya@rkmvu.ac.in

† pedroferreira@usp.br

‡ devashibhai.adroja@stfc.ac.uk

§ luizeleno@usp.br

- [1] F. B. Santos, L. E. Correa, B. S. de Lima, O. V. Cigarroa, M. S. da Luz, T. W. Grant, Z. Fisk and A. J. S. Machado, Phys. Lett. A **382**, 1065 (2018).
- [2] J. E. Sonier, J. H. Brewer, and R. F. Kiefl, Rev. Mod. Phys. **72**, 769 (2000).
- [3] E. H. Brandt, Phys. Rev. B **68**, 054506 (2003).
- [4] E. E. Chia, M. Salamon, H. Sugawara, and H. Sato, Phys. Rev. B **69**, 180509 (2004).
- [5] A. Amato, Rev. Mod. Phys. **69**, 1119 (1997).
- [6] W. L. McMillan, Phys. Rev. **167**, 331 (1968).
- [7] A. Bhattacharyya, D. T. Adroja, P. K. Biswas, Y. J. Sato, M. R. Lees, D. Aoki, and A. D. Hillier, J. Phys. Cond. Matter, at press (2019).
- [8] D. Das, R. Gupta, A. Bhattacharyya, P. K. Biswas, D. T. Adroja, and Z. Hossain, Phys. Rev. B **97**, 184509 (2018).
- [9] A.H. Hillier and R. Cywinski, Applied Magnetic resonance, **13**, 95 (1997).
- [10] Y J Uemura, G M Loke, B J Sternlieb, J H Brewer, J F Carolan, W N Hardy, R Kadono, J R Kempton, R F Kiefl, S R Kreitzman, P Mulhern, T M Riseman, D Ll Williams, B X Yang, S Uchida, H Takagi, J Gopalkrishnan, A W Sleight, M A Subramanian, C L Chien, M Z Cieplak, Gang Xiao, V Y Lee, B W Statt, C E Stronach, W J Kossler and X H Yu, Phys. Rev. Lett. **62**, 2317 (1989).
- [11] P. Ferreira, F. Santos, A. Machado, H. Petrilli, and L. Eleno, Physical Review B **98**, 045126 (2018).

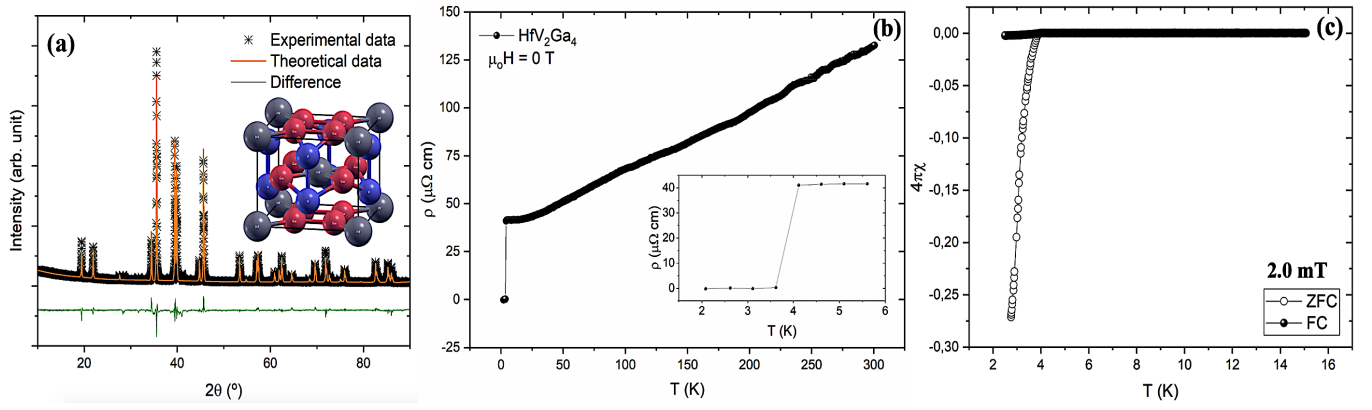


FIG. 4. (a) Represent the X-ray diffraction pattern (symbols) of HfV_2Ga_4 with Rietveld refinement (solid red line). Inset of (a) shows the tetragonal unit cell of HfV_2Ga_4 , where Hf (gray), V (blue), and Ga (red) occupy at the $2a$ $(0, 0, 0)$, $4d$ $(0, \frac{1}{2}, \frac{1}{4})$, and $8h$ $(0.303, 0.303, 0)$ Wyckoff positions, respectively. (b) Temperature variation of resistivity over the range $1.8 \text{ K} \leq T \leq 300 \text{ K}$, with the inset showing a drop in the resistivity at 3.9 K. (c) Temperature dependence of the magnetic susceptibility $\chi(T)$ in zero-field-cooled warming and field-cooled cooling (FCC) mode in presence of an applied magnetic field of 2 mT.

TABLE I. The parameters obtained from the fit to the $\sigma_{sc}(T)$ data of HfV_2Ga_4 using different gap models.

Model	$g(\phi)$	Gap Value $\Delta(0)$ (meV)	Gap Ratio $2\Delta(0)/k_B T_C$	Weight factor	χ^2
$s + d$ -wave	$1, \cos(2\phi)$	0.98(1); 0.09(6)	6.27(2); 1.14(1)	0.57(1)	1.3(2)
$s + s$ -wave	1	1.08(3); 0.09(7)	6.91(1); 0.57(5)	0.87(2)	2.2(3)
anisotropy s -wave	$\frac{ 1+\cos(\phi) }{2}$	1.14(2)	7.29(2)	1.0	2.3(1)
s -wave	1	0.91(4)	5.84(1)	1.0	2.3(2)
d -wave	$\cos(2\phi)$	9.78(7)	2.82(1)	1.0	3.0(3)

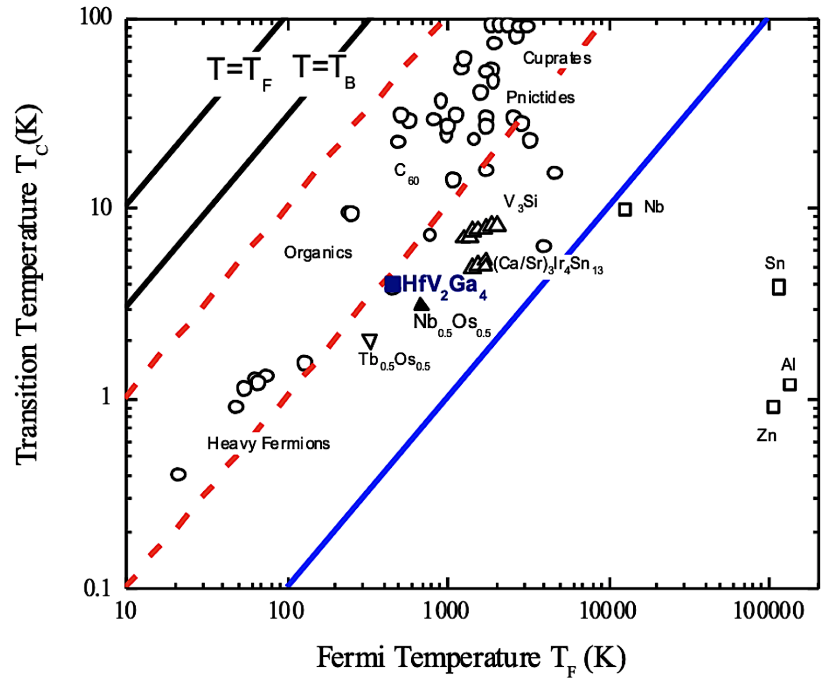


FIG. 5. (Color online) A schematic description of the Uemura plot. The exotic superconductors fall within a universal band for which $1/100 < T_C/T_F < 1/10$, shown by the area between two red colors dashed lines in the figure. The solid black line resembles the Bose-Einstein condensation temperature (T_B). [9]

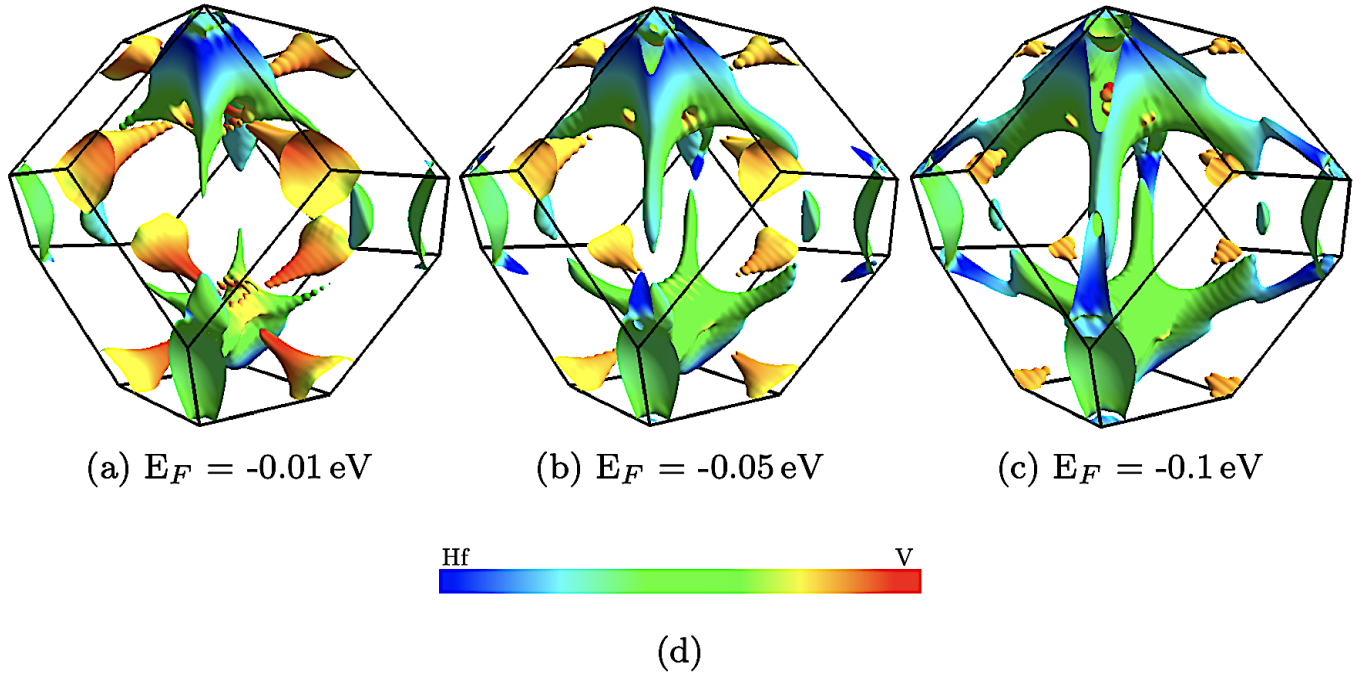


FIG. 6. Evolution of the orbital character projected over the Fermi surface, with hole doping according to the rigid band approximation.